Research Paper

Scavenger Receptor-Mediated Targeted Treatment of Collagen-Induced Arthritis by Dextran Sulfate−Methotrexate Prodrug

Modi Yang[1,3], Jianxun Ding[1,✉], Xiangru Feng[1], Fei Chang[2,✉], Yinan Wang[4], Zhongli Gao[3], Xiuli Zhuang[1], and Xuesi Chen[1]

1. Key Laboratory of Polymer Ecomaterials, Changchun Institute of Applied Chemistry, Chinese Academy of Sciences, Changchun 130022, P. R. China;
2. Department of Orthopedics, The Second Hospital of Jilin University, Changchun 130041, P. R. China;
3. Department of Orthopedics, China-Japan Union Hospital of Jilin University, Changchun 130033, P. R. China;
4. Institute of Immunology, Academy of Translational Medicine, First Hospital of Jilin University, Changchun 130021, P. R. China.

✉ Corresponding authors: Jianxun Ding, E-mail: jxding@ciac.ac.cn; Fei Chang, E-mail: ccfei_cn@hotmail.com.

Abstract

Rheumatoid arthritis (RA) is a chronic autoimmune disorder implicated in multiple joint affection and even disability. The activated macrophages perform a predominant role in onset and persistence of RA. Scavenger receptor (SR), one of several receptors overexpressed on the activated macrophages, is a specific biomarker for targeted therapy of numerous chronic inflammation diseases like RA. In this work, dextran sulfate-*graft*-methotrexate conjugate (DS-*g*-MTX) is synthesized and characterized, which exhibits excellent targetability to SR on the activated RAW 264.7 cells. Additionally, the enhanced accumulation and potent inflammatory inhibition are observed in the affected joint after intravenous injection of DS-*g*-MTX, compared to the treatment with dextran-*graft*-methotrexate (Dex-*g*-MTX), as is confirmed by the detection of histopathology and pro-inflammatory cytokines. Our work highlights DS-*g*-MTX as a potential therapeutic option for RA aiming the SR-expressed activated macrophages.

Key words: collagen-induced arthritis, controlled release, scavenger receptor, methotrexate prodrug, rheumatoid arthritis therapy.

Introduction

Rheumatoid arthritis (RA) is a chronic systemic autoimmune disease mainly characterized by hyperplastic synovium, persistent synovitis, injuries of joints and articular cartilage, *etc.* [1-4]. Over 70 million cases of RA are estimated to occur worldwide annually, and patients might have to suffer from multiple systematic complications, and even physical disability [2, 5]. In the pathological process of RA, the activated macrophages prolong inflammatory period and exacerbate the affected joints [6], attributed to the release of inflammatory cytokines and the differentiation into osteoclasts [7]. Macrophages are the main source of varied inflammatory cytokines, such as tumor necrosis factor-α (TNF-α), interleukin-1β (IL-1β), interleukin-6 (IL-6), and so on.

These cytokines are actively involved in inflammation process, immune activity, and metabolism of cartilage and bone [6]. Consequently, the activated macrophages make a suitable candidate for targeted therapy of RA.

As a predominant cell population in the synovium of RA [8], the activated macrophages are mainly located at inflamed sites in RA. Scavenger receptor (SR) is a member of glycoproteins expressed on the surface of macrophages that combines with the ligands of serum albumin, polyanionic macromolecules, and oxidized low-density lipoprotein (LDL) in the inflamed microenvironment [9]. Recently, there is an increasing interest in the study associated with the targeted therapy of RA by

SR. Hemoglobin SR (HbSR), also named CD163, is specifically overexpressed on the membrane of monocyte-macrophages in the inflammatory microenvironment. It was reported that the uptake of liposome by macrophages was significantly enhanced by the linkage of CD163-monoclonal antibody to liposome [10]. The use of doxorubicin (DOX) resulted in stronger cytotoxicity toward human monocytes, thus the expression of HbSR was subsequently inhibited. In another study, CD163-monoclonal antibody conjugating dexamethasone (DXM) showed a 50-fold increase in anti-inflammation efficacy and significantly reduced side effects *versus* free dexamethasone [11]. Dextran sulfate (DS) is a hydrophilic polysaccharide that selectively binds to class A of SR *via* ligand-receptor recognition [12]. An amphiphilic block copolymer composed of DS and poly(ε-caprolactone) (PCL, a hydrophobic block) was synthesized according to a published report [13]. Systematic *in vitro* and *in vivo* studies demonstrated that the copolymer possessed the ability to target the activated macrophages and selectively accumulate in the affected joints of collagen-induced arthritis (CIA) mice *via* passive and/or active targeting strategies. Therefore, DS becomes a useful ligand toward SR on the activated macrophages for targeted therapy of RA.

Nanocarriers features many advantages, such as specific accumulation at the target sites, prolonged circulation kinetics, sustained release, and increased efficacy with reduced toxicity at low dose [14]. Thus, the employment of nanoscale drug delivery system may be necessary to overcome the defects of current therapeutic regimens of RA [15]. Methotrexate (MTX) was a widely used cytotoxic agent for chemotherapy of malignancies yet now is a first-line conventional drug for RA therapy. However, severe drug resistance and multiple adverse effects of MTX have long been hampering the long-term use of this agent [16, 17]. Therefore, directing drugs to inflamed sites and reducing distribution in unwanted organs may readily solve these problems.

In this work, we engineered a macrophage-targeted dextran sulfate−methotrexate conjugate (DS-*g*-MTX) as well as an untargeted dextran−methotrexate prodrug (Dex-*g*-MTX) through condensation reaction. Subsequently, confirmations of chemical structures, self-assembled behaviors, and drug release behaviors were investigated. Further, we tested the targetability and cytotoxicity of both MTX-conjugated micelles toward the activated and unactivated macrophages *in vitro*. Evaluation of biodistribution and therapeutic efficacy *in vivo* was carried out in CIA mice. Finally, the analyses of histopathology and pro-inflammatory cytokines were performed for assessment of anti-inflammation efficacy of DS-*g*-MTX and Dex-*g*-MTX.

Results and Discussion

Syntheses and Characterizations of Conjugates

As shown in Scheme 1, both DS-*g*-MTX and Dex-*g*-MTX were synthesized by condensation reaction with 1-ethyl-(3-(dimethylamino)propyl) carbodiimide hydrochloride (EDC·HCl) as a condensing agent and 4-*N*,*N*-dimethylaminopyridine (DMAP) as a catalyst. As depicted in proton nuclear magnetic resonance (^{1}H NMR) spectra (Supplementary Figure S1), the signals of 8.53 ppm (a), 7.64 ppm (b), and 6.84 ppm (c) were the characteristic peaks of aromatic protons in MTX, suggesting the successful syntheses of both DS-*g*-MTX and Dex-*g*-MTX. In Fourier-transform infrared (FT-IR) spectra, as shown in Supplementary Figure S2, the signals of carboxyl group in MTX were found at 1605 and 1640 cm^{-1}, yet were not shown in prodrugs, indicating the expected reaction between DS/Dex and MTX. The MTX contents of DS-*g*-MTX and Dex-*g*-MTX were determined to be 3.9 and 4.2 wt.% by ultraviolet-visible (UV-Vis) spectrophotometer.

DS-*g*-MTX and Dex-*g*-MTX self-assembled in aqueous solution due to the amphiphilic property. As shown in Figure 1A and 1C, both DS-*g*-MTX and Dex-*g*-MTX micelles clearly showed spherical morphologies. The mean diameters of DS-*g*-MTX and Dex-*g*-MTX were approximately 95 and 90 nm tested by transmission electron microscopy (TEM), respectively. In Figure 1B and 1D, the hydrodynamic diameters (D_hs) of DS-*g*-MTX and Dex-*g*-MTX micelles were 104.4 ± 14.4 and 94.0 ± 22.0 nm by dynamic laser scattering (DLS), respectively, which were slightly higher than those measured by TEM for the aqueous condition of DLS. The suitable diameters of the two micelles (~ 100 nm) enabled them to selectively accumulate in inflamed areas *via* the enhanced permeability and retention (EPR) effect. The EPR effect allows nanovehicles with certain sizes to pass through the leaky vascular and accumulate in tumor tissue more than they do in normal tissues [18, 19].

As shown in Supplementary Figure S3, the CMCs of DS-*g*-MTX and Dex-*g*-MTX micelles were acquired with the fluorescence intensity of Nile Red being the probe. Practically, the CMCs were calculated from the first inflection point in the sigmoidal curve. The CMCs of DS-*g*-MTX and Dex-*g*-MTX micelles were 4.53×10^{-2} and 0.21 mg/mL, respectively, far below the treatment concentration, thus the formation of the two micelles was ensured.
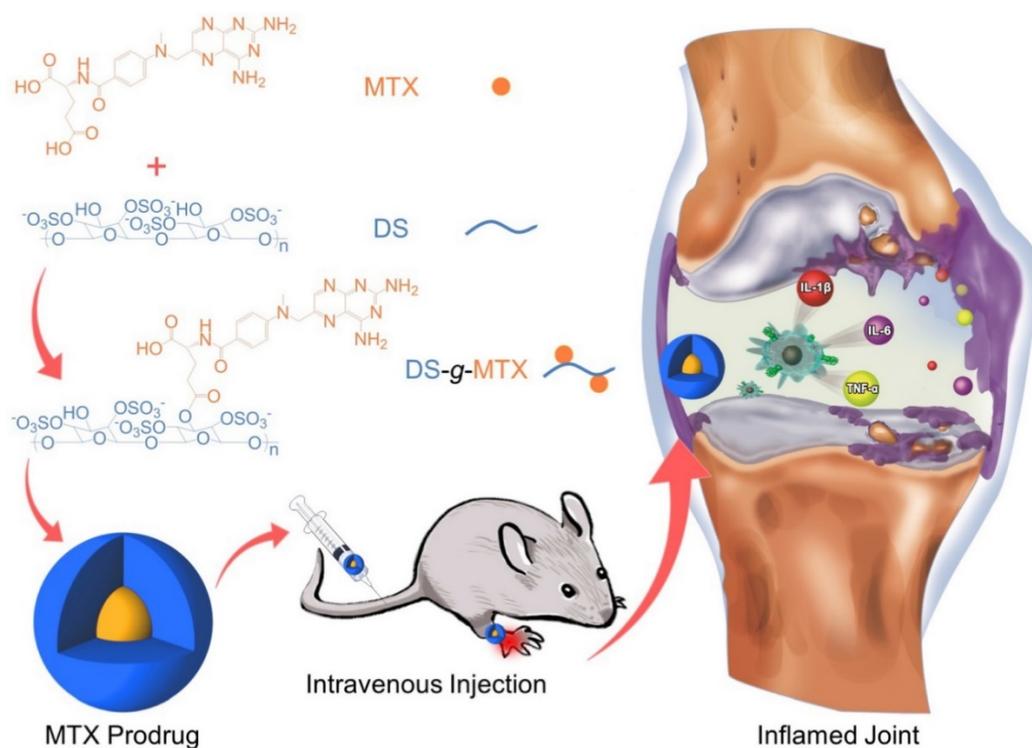
Scheme 1. Schematic illustration of synthesis, self-assembly, administration, and selective accumulation of DS-*g*-MTX in CIA model.
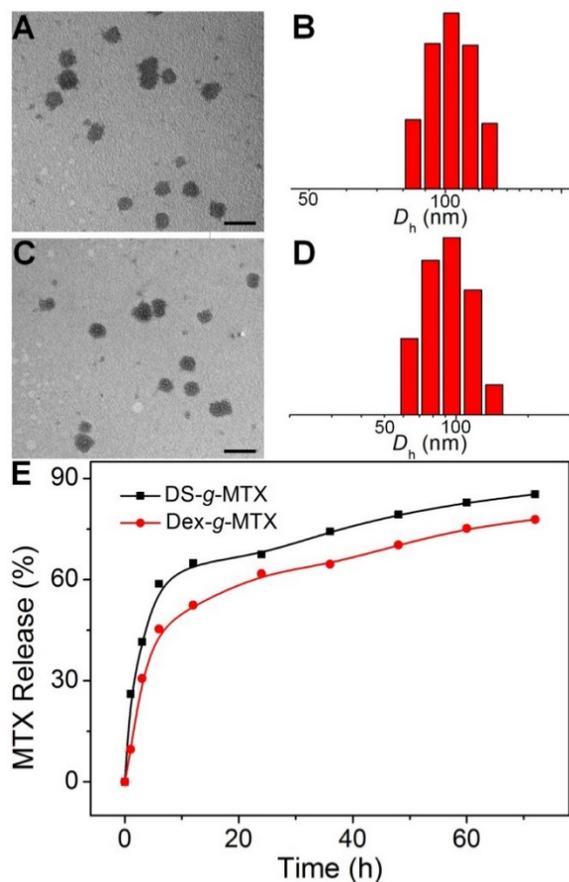
Figure 1. Typical TEM microimages (A and C) and D_hs (B and D) of DS-*g*-MTX (A and B) and Dex-*g*-MTX (C and D). MTX release profiles of DS-*g*-MTX and Dex-*g*-MTX in PBS of pH 7.4 at 37 °C (E). Scale bars: 200.0 nm.

Biocompatibility test is a key preclinical evaluation of a new drug before application *in vivo* [20]. Herein, hemolysis was conducted as an effective method frequently used for hemocompatibility evaluation. Hemolysis is a phenomenon of red blood cell lysis and hemoglobin discharge caused by varied physiochemical factors. Therefore, a drug proved to trigger hemolysis will most probably be rejected to be administrated *in vivo*. In this study, the biocompatibility of DS-*g*-MTX and Dex-*g*-MTX was detected through spectroscopy on the basis of the published work [21]. As shown in Supplementary Figure S4, no hemolysis was found in any groups of DS-*g*-MTX or Dex-*g*-MTX, confirming favorable biocompatibility.

Sustained Drug Release and Upregulated Cytotoxicity *In Vitro*

The *in vitro* MTX release was carried out in PBS at pH 7.4 (Figure 1E). The level of MTX release from DS-*g*-MTX was slightly higher than Dex-*g*-MTX during the whole process. At 72 h, 84.15% of the total MTX in DS-*g*-MTX was released and 77.68% in DS-*g*-MTX. No significant burst release was observed in either group. The result was in accordance with the distinct structures of two micelles. The electric charge of DS endowed DS-*g*-MTX micelle with looser construction, which facilitated the release of MTX from the prodrug.
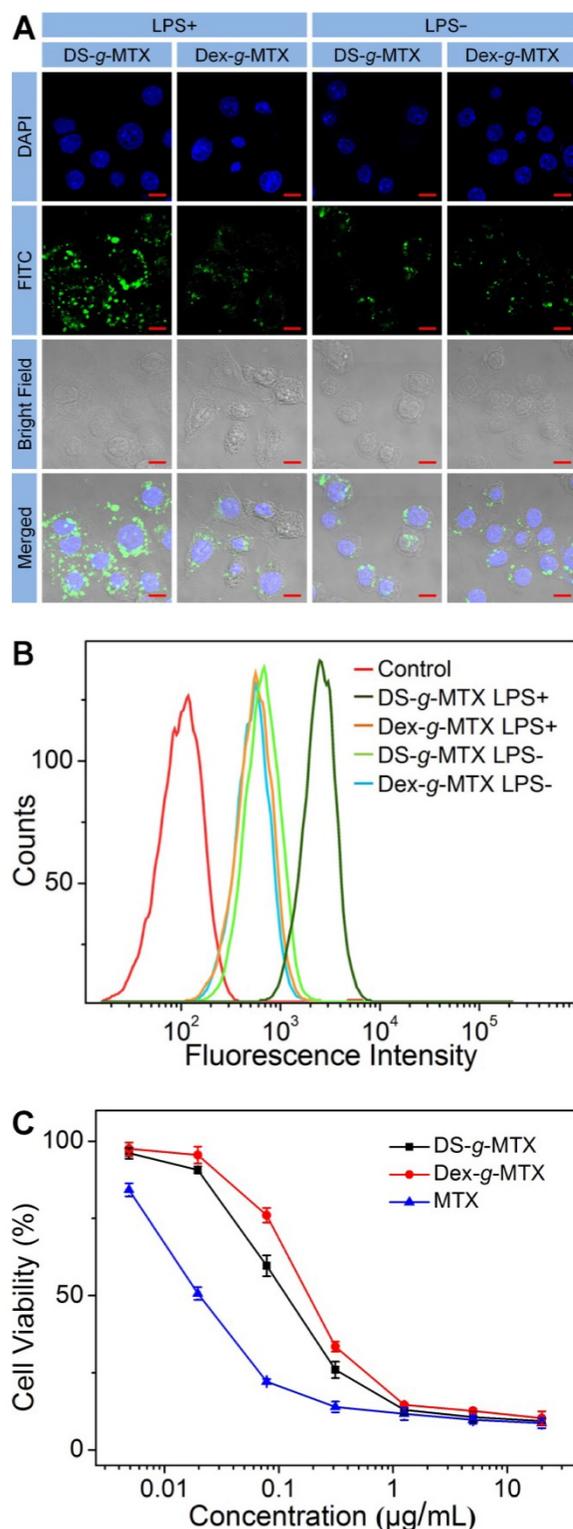
Figure 2. CLSM microimages (A) and FCM results (B) of RAW 264.7 cells incubated with FITC-labled DS-*g*-MTX or Dex-*g*-MTX for 2 h after activited by LPS (+) or not (−). Cells of the control group were incubated with PBS. Scale bars: 10.0 μm. Cytotoxicity of DS-*g*-MTX, Dex-*g*-MTX, and free MTX after coincubation for 72 h toward RAW 264.7 cells activated by LPS *in vitro* (C). Data were presented as mean ± standard deviation (SD; *n* = 3).

As shown in Figure 2A, the targetability of DS-*g*-MTX and Dex-*g*-MTX toward the activated and

unactivated RAW 264.7 cells was evaluated by confocal laser scanning microscopy (CLSM). The strongest fluorescence signal was detected in the activated RAW 264.7 cells treated with DS-*g*-MTX. In the activated cells, the intracellular internalization of DS-*g*-MTX was remarkably enhanced in comparison with Dex-*g*-MTX. Little difference was detected between DS-*g*-MTX and Dex-*g*-MTX in the unactivated cells due to the rare expression of SR. Subsequently, FCM was carried out to confirm the trend of cellular uptake of DS-*g*-MTX and Dex-*g*-MTX. Figure 2B showed that DS-*g*-MTX was more prone to be taken into the activated macrophages than Dex-*g*-MTX. However, the fluorescence intensity of DS-*g*-MTX and Dex-*g*-MTX was equally less obvious toward unactivated macrophages, in accordance with the previous test.

The cytotoxicity of the two conjugates was measured by methyl thiazolyl tetrazolium (MTT) tests. RAW 264.7 cells activated by lipopolysaccharide (LPS) were adopted. As illustrated in Supplementary Figure S5, no cytotoxicity was observed in the activated or unactivated RAW 264.7 cells treated with Dex and DS. The results excluded the impact of the efficacy for CIA of pure polysaccharides. In Figure 2C, DS-*g*-MTX featured the augmented cellular uptake compared with Dex-*g*-MTX due to the specific recognition of DS to SR overexpressed on the membrane of activated macrophages, resulting in severer cytotoxicity. As expected, free MTX showed significantly higher degree of toxicity toward RAW 264.7 cells than the two conjugates.

SR overexpressed on the activated macrophages mainly mediated the cellular uptake of DS-*g*-MTX. High affinity of DS toward SR accounted for its favorable intracellular internalization and targetability. On the contrary, in the unactivated macrophages where scarce SR was expressed, the intracellular internalization of both groups was largely harnessed. Consequently, DS-*g*-MTX exhibited promising targetability and cytotoxicity toward the activated macrophages *in vitro*.

Selective Biodistribution *In Vivo*

The biodistribution is a pivotal issue with regard to the therapeutic efficacy as well as the adverse effects of a new nanoscale drug [22]. In this work, CIA mice were injected *i.v.* with DS-*g*-MTX, Dex-*g*-MTX, and MTX at 48 days after the primary immunization with normal saline (NS) as a control. At 12 h post-injection, the hind limbs were isolated, and the fluorescence images were conducted by a Maestro 500FL *in vivo* Imaging System (Cambridge Research & Instrumentation, Inc., USA). As can be seen from Figure 3A, a much higher level of DS-*g*-MTX

accumulated at inflamed site than Dex-*g*-MTX and free MTX, suggesting the improved selectivity, whereas the control group showed minimal accumulation. To further investigate the biodistribution of different MTX formulations, the semi-quantitative analysis of fluorescence signal was carried out (Figure 3B). The graph illustrated a similar pattern as fluorescence images. The results proved that the nanoscale drug delivery system in proper size could preferably accumulate in inflammatory area [23]. DS-*g*-MTX and Dex-*g*-MTX with a diameter of around 100 nm could effectively locate in the inflamed joints *via* the EPR effect instead of being rapidly eliminated by reticuloendothelial system (RES) [18]. Furthermore, in terms of biodistribution of the two conjugates, favorable accumulation in the affected joint was detected *via* intravenous injection of DS-*g*-MTX, which may be due to the specific bond between DS and SR overexpressed on the activated macrophages. Promising biodistribution of DS-*g*-MTX was demonstrated by passive and active targetability ensuring that fewer drugs would circulate to the untargeted organs; therefore, adverse effects would be enormously averted. Our work suggested that excellent targetability and biodistribution was obtained by intravenous administration of DS-*g*-MTX.
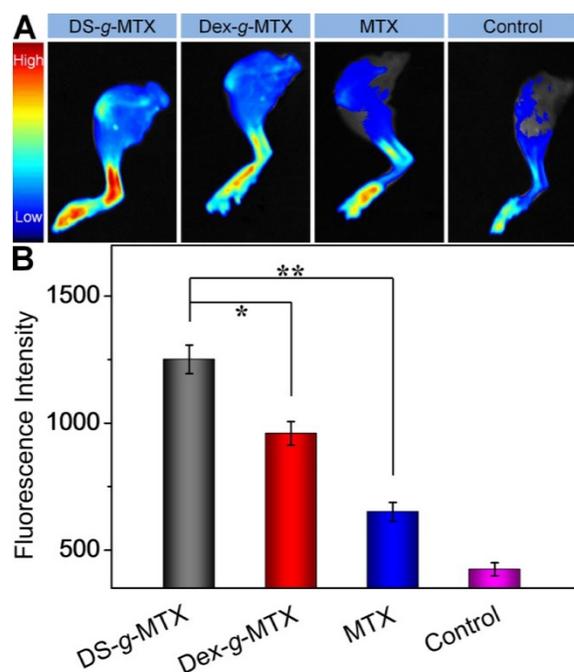
Figure 3. *Ex vivo* FITC fluorescence images of affected joints (A) and average signals detected from ankle joints (B) of CIA mice treated with DS-*g*-MTX, Dex-*g*-MTX, free MTX, or NS as a control. Data were presented as mean ± SD (*n* = 3; *P < 0.05, **P < 0.01).

Therapeutic Efficacies of CIA Models

To evaluate the therapeutic efficacies of DS-*g*-MTX and Dex-*g*-MTX, a CIA animal model was induced in DBA/1J mice. At 30 days after primary immunization, DS-*g*-MTX, Dex-*g*-MTX, and free MTX at a MTX equivalent dose of 5.0 mg per kg body weight (mg/(kg BW)), and NS as a control were intravenously administrated every 3 days. The clinical scores and hind paw thicknesses were measured prior to every injection. The last measurement was conducted at 3 days after the last injection, and photographs were taken at the same time. In Figure 4A, the control group suffered significant erythema and swelling in the paw, while the signs were markedly alleviated in the DS-*g*-MTX and Dex-*g*-MTX group, with a more satisfactory inhibition of inflammation in the DS-*g*-MTX group. Free MTX was hardly effective in respect of erythema and swelling. Similar phenomenon was observed as shown in Figure 4B, where the arthritic score of control group peaked at 11 at the last measurement day, representing the worse state of all groups.
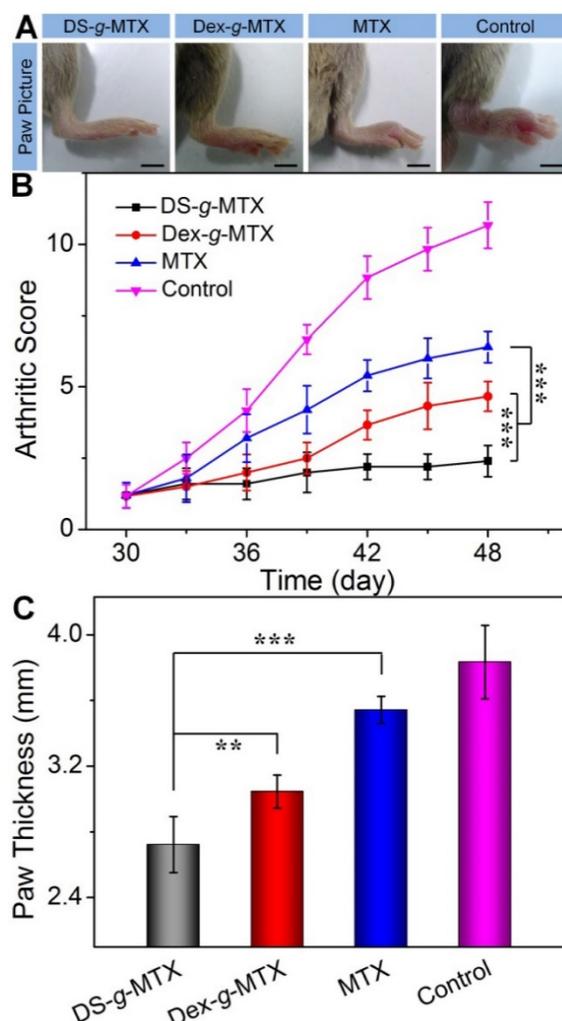
Figure 4. Macroscopic images of inflamed joints from CIA mice treated with DS-*g*-MTX, Dex-*g*-MTX, free MTX, or NS as a control after 3 days of last injection (A). The macroscopic evidences of arthritis were assessed by arthritic sores in the process of treatment (B) and paw thickness after all treatments (C). Data were presented as mean ± SD (*n* = 6; **P < 0.01, ***P < 0.001). Scale bars: 5.0 mm.
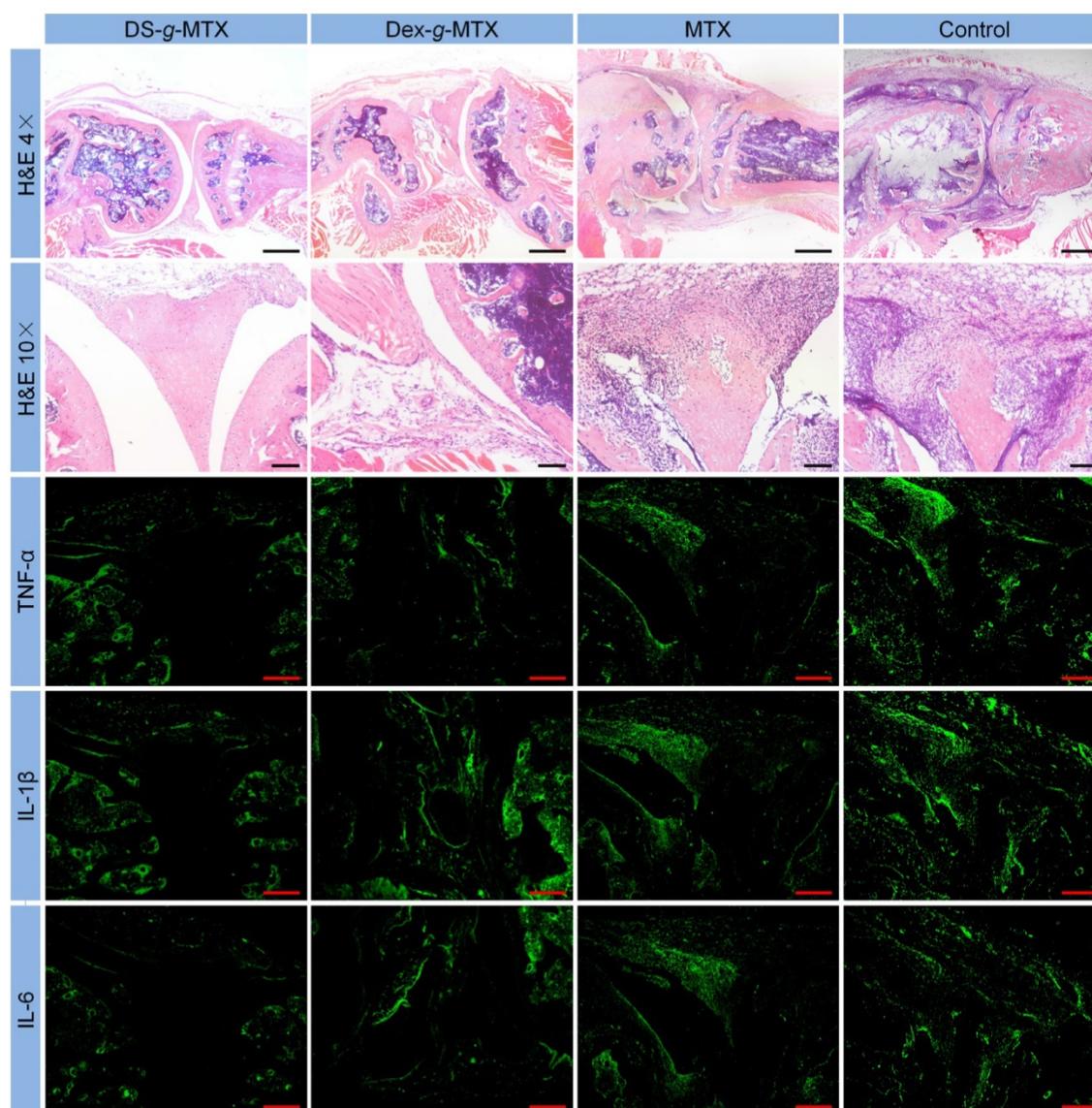
Figure 5. Microimages of H&E staining and immunofluorescence analyses (*i.e.*, TNF-α, IL-1β, and IL-6) of affected joints using continuous sections. Scale bars in H&E (4×): 500.0μm; scale bars in H&E (10×) and immunofluorescence: 200.0 μm.

The overall condition of inflammatory site was noticeably improved in the DS-*g*-MTX group, significantly better than that of the Dex-*g*-MTX group ($P < 0.001$). To further confirm the therapeutic efficacy of the conjugates, the average hind paw thickness was measured as an indicator of arthritic symptom (Figure 4C). The figures of DS-*g*-MTX, Dex-*g*-MTX, free MTX, and control group were 2.72, 3.05, 3.54, and 3.83 mm, respectively, in accordance with the previous results in Figure 4A and 4B. The treatment of DS-*g*-MTX exhibited the most remarkable inhibitory efficacy on arthritic inflammation attributed to the passive and active targeting effects. As a comparison, Dex-*g*-MTX showed less efficiency for it mostly depended on the EPR effect alone. Consequently, with targetability and suitable size for the EPR effect, DS-*g*-MTX endowed great potential as an excellent mode for targeted therapy of RA.

Histopathological Analyses

Histopathological analyses of knee joints were carried out in order to assess the anti-inflammation efficiency of varied MTX formulations. Three joints of every group were analyzed for histopathology. As shown in Figure 5, inflammatory cells stained blue invaded into the hyperplastic synovium, filled up the joint space, and spread on the surface of articular cartilage. The joint space became increasingly narrow, while the articular cartilage, eroded by pro-inflammatory cytokines and proteinases, was rough and thin. Comparatively speaking, there existed fewer inflammatory regions in the images of DS-*g*-MTX and Dex-*g*-MTX. Moreover, the morphology of articular cartilage remained almost

integral, showing that both conjugates inhibited the recruitment of inflammatory cells. Despite the impressive capability of Dex-*g*-MTX in anti-inflammation, hyperplasia of synovium and a bit erosion of articular cartilage were clearly observed. As listed in Supplementary Tables S1 and S2, HSS (histopathological scores of synovium) and modified OARSI (Osteoarthritis Research Society International) scores further confirmed the results. As expected, the HSS and modified OARSI scores of control group were much higher than the two MTX conjugates groups (Figure S6A and S6B). Both DS-*g*-MTX and Dex-*g*-MTX groups proved to effectively inhibit synovitis and protect articular cartilage, when DS-*g*-MTX showed a more remarkable effect. A certain extent of anti-inflammation function can also be detected in free MTX.

Pro-inflammatory Cytokines Assays

To further confirm the anti-inflammation efficacies of various MTX formulations mentioned above, pro-inflammatory cytokines assays including immunofluorescence, enzyme-linked immunosorbent assay (ELISA) assays, and real-time reverse transcriptase polymerase chain reaction (RT-PCR) tests were carried out in this work. Three joints of every group were analyzed for immunofluorescence, RT-PCR, and ELISA tests. Pro-inflammatory cytokines including TNF-α, IL-1β, and IL-6 are crucial indicators for the pathological processes of RA [24, 25]. Among multiple cytokines, TNF-α is an influential factor in stimulating secretion of various pro-inflammatory cytokines, thus is widely involved in the proliferation of synovial fibroblasts, activation of osteoblasts, and destruction of cartilage and bone [26, 27]. IL-1β belongs to IL-1 family. It induces cartilage metabolic disorder, bone absorption, and synovitis *via* promoting the release of other pro-inflammatory cytokines and proteinases, in the meantime down-regulates proteoglycan synthesis [8, 28-30]. IL-6 is involved in activation of synovial fibroblasts and osteoblasts, leading to articular cartilage and bone erosion [31, 32]. Immunofluorescence analyses of continuous pathological sections were conducted to compare the cytokines expression in inflamed joints treated with different MTX formulations.

As shown in Figure 5, most cytokines stored up in hyperplastic synovium, coinciding with the result in the H&E-stained microimages. As expected, a significant increase in the secretion of TNF-α, IL-1β, and IL-6 was seen in the joints of control group, whereas CIA mice administrated with DS-*g*-MTX showed a remarkably reduced expression of these cytokines. Some extent of inhibition effect was also detected in the Dex-*g*-MTX and free MTX group. To further confirm our findings, the relative expression areas of the three pro-inflammatory cytokines above were analyzed by ImageJ software (National Institutes of Health, Bethesda, Maryland, USA). As shown in Supplementary Figure S6C, S6D, and S6E, the expression relative areas of TNF-α, IL-1β, and IL-6 were the lowest in the DS-*g*-MTX group, that is, 4.55, 5.65, and 3.01%, respectively, representing the most remarkable secretion inhibition of pro-inflammatory cytokines. The inhibition effect of Dex-*g*-MTX was relatively lower than that of DS-*g*-MTX (TNF-α: $P <$ 0.01, IL-1β: $P < 0.001$, and IL-6: $P < 0.001$). Reasonably, the NS-treated mice possessed the largest expression relative area, representing the most serious synovitis and cartilage erosion. No distinct difference was detected between free MTX group and control group ($P > 0.05$). The above data validated that significant suppression of synovitis and excellent protection of cartilage against erosion were obtained due to the powerful expression inhibition of pro-inflammatory cytokines from the treatment of DS-*g*-MTX.

To further confirm the suppression ability of various MTX conjugates toward pro-inflammatory cytokines *in situ*, relative mRNA expressions of TNF-α, IL-1β, and IL-6 in the inflamed joints were measured by RT-PCR. As shown in Figure 6A, 6C, and 6E, the DS-*g*-MTX group exhibited the lowest relative mRNA expression of all three pro-inflammatory cytokines among all groups. Combined with the result of immunofluorescence, mRNA test further confirmed that DS-*g*-MTX effectively down-regulated the expression of pro-inflammatory cytokines due to selective biodistribution and significant targetability to the activated macrophages, which served as a main source of pro-inflammatory cytokines.

Furthermore, we detected the serum concentrations of pro-inflammatory cytokines as crucial indexes of therapeutic efficacy. Consequently, the concentrations of TNF-α, IL-1β, and IL-6 in serum were tested by the commercial ELISA kits. As shown in Figure 6B, 6D, and 6F, the expression of the three pro-inflammatory cytokines was largely stimulated in the control and free MTX groups, while the two MTX conjugates showed different extents of suppression. In accordance with immunofluorescence images and mRNA detections, the concentrations of TNF-α, IL-1β, and IL-6 in serum were the lowest in the DS-*g*-MTX group, which was 27.8, 33.3, and 33.3% of those in the control group. Therefore, DS-*g*-MTX could dominate reduction of the levels of pro-inflammatory cytokines both in the affected joints and serum. The finding was shown on account of the passive and active targeting properties of DS-*g*-MTX. By reducing the level of

pro-inflammatory cytokines in the affected joints, DS-*g*-MTX manifested excellent inhibition of synovitis and cartilage erosion, acting as an efficient macrophage-targeted drug for RA therapy.

Conclusion

In this work, the macrophage-targeted DS-*g*-MTX and untargeted Dex-*g*-MTX as a control were synthesized for treatment of RA. The two conjugates with precise chemical structures self-assembled into spherical micelles of around 100 nm in diameter under the physiological environment, which was suitable for passive targeting delivery into the affected joints through the EPR effect. In addition, DS-*g*-MTX could selectively target to the activated macrophages, which resulted from the specific recognition of DS to SR. Therefore, compared with Dex-*g*-MTX and free MTX, DS-*g*-MTX showed less cytotoxicity to normal cells, more selective biodistribution, and stronger anti-inflammation effect in the inflamed area. Furthermore, DS-*g*-MTX group led to significant alleviation of synovitis and protection of articular cartilage by inhibiting the expression of pro-inflammatory cytokines. Finally, the macrophage-targeted prodrug, that is, DS-*g*-MTX, showed great potential for targeted treatment of RA.

As is widely believed, the cell-targeted polymer conjugates hold broad prospect in the targeted treatment of RA. An increasing amount of prodrugs will be developed and tested to gain excellent clinical outcome. In the future, drugs designed *via* nanotechnology may prevent patients from synovitis, articular cartilage, bone erosion, and even joint replacement.
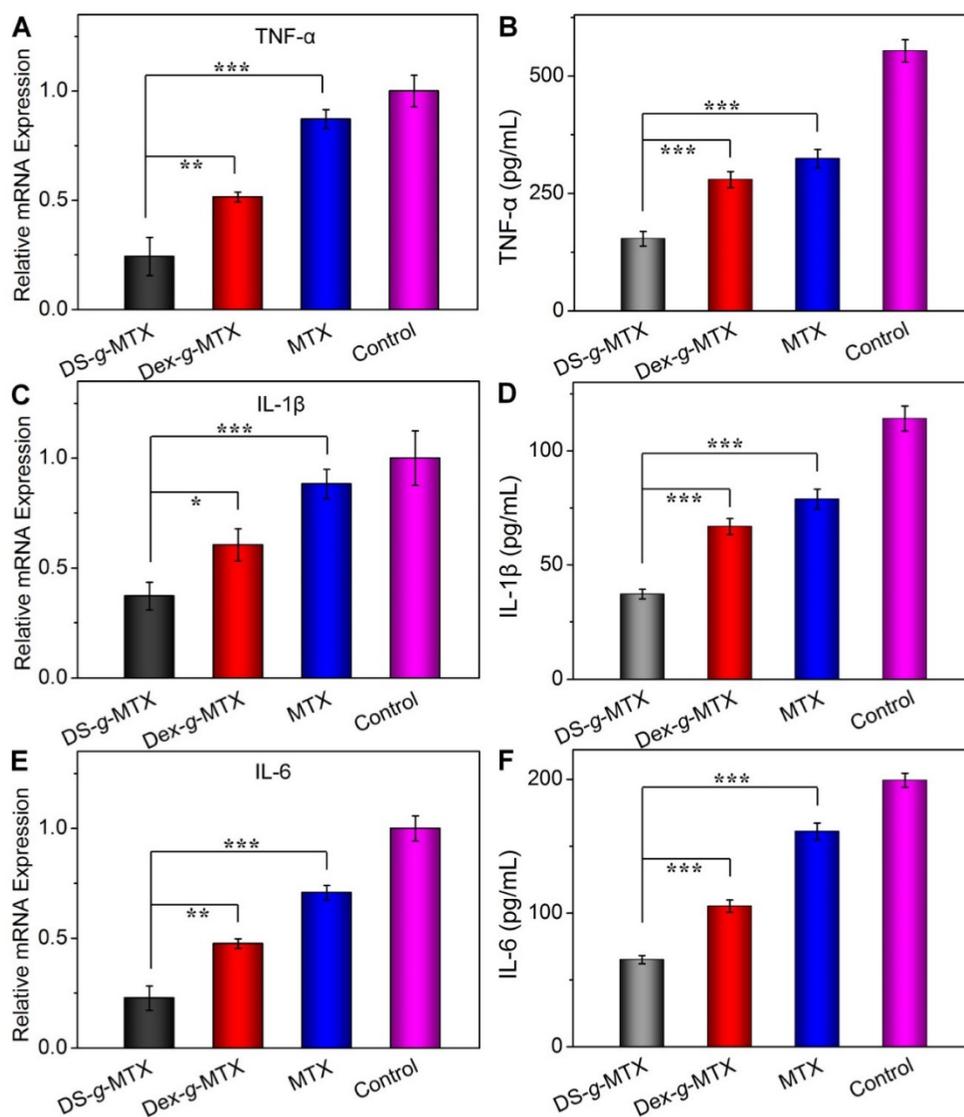
Figure 6. Serum concentrations and relative mRNA expression of pro-inflammatory cytokines, *i.e.*, TNF-α (A and B), IL-1β (C and D), and IL-6 (E and F) in DS-*g*-MTX, Dex-*g*-MTX, free MTX, and NS as control groups were measured by ELISA and RT-PCR tests. Data were presented as mean ± SD (n = 3; *P < 0.05, **P < 0.01, ***P < 0.001).

Supplementary Material

Supplementary tables and figures. Supplementary materials and methods; Supplementary ¹HNMR and FI-TC spectra, CMCs, and hemolysis of MTX prodrugs; Supplementary HSS and modified OARSI scores after treatments with various MTX formulations; Supplementary score standards of morphological features of synovium and modified OARSI; Supplementary primer sequences for RT-PCR. http://www.thno.org/v07p0097s1.pdf

Acknowledgements

Competing Interests

The authors have declared that no competing interest exists.

References

1. Firestein GS. Evolving concepts of rheumatoid arthritis. Nature. 2003; 423: 356-61.
2. Scott DL, Wolfe F, Huizinga TW. Rheumatoid arthritis. Lancet. 2010; 376: 1094-108.
3. Liu H, Ding J, Wang C, Wang J, Wang Y, Yang M, et al. Intra-Articular Transplantation of Allogeneic BMMSCs Rehabilitates Cartilage Injury of Antigen-Induced Arthritis. Tissue Eng Part A. 2015; 21: 2733-43.
4. Liu H, Ding J, Wang J, Wang Y, Yang M, Zhang Y, et al. Remission of Collagen-Induced Arthritis through Combination Therapy of Microfracture and Transplantation of Thermogel-Encapsulated Bone Marrow Mesenchymal Stem Cells. PLoS ONE. 2015; 10: e0120596.
5. Smolen JS, Steiner G. Therapeutic strategies for rheumatoid arthritis. Nat Rev Drug Discov. 2003; 2: 473-88.
6. McInnes IB, Schett G. The Pathogenesis of Rheumatoid Arthritis. New Engl J Med. 2011; 365: 2205-19.
7. Davignon JL, Hayder M, Baron M, Boyer JF, Constantin A, Apparailly F, et al. Targeting monocytes/macrophages in the treatment of rheumatoid arthritis. Rheumatology. 2013; 52: 590-8.
8. Kinne RW, Stuhlmuller B, Burmester GR. Cells of the synovium in rheumatoid arthritis. Macrophages. Arthritis Res Ther. 2007; 9: 224.
9. Jain NK, Mishra V, Mehra NK. Targeted drug delivery to macrophages. Expert Opin Drug Del. 2013; 10: 353-67.
10. Etzerodt A, Maniecki MB, Graversen JH, Møller HJ, Torchilin VP, Moestrup SK. Efficient intracellular drug-targeting of macrophages using stealth liposomes directed to the hemoglobin scavenger receptor CD163. J Control Release. 2012; 160: 72-80.
11. Graversen JH, Svendsen P, Dagnaes-Hansen F, Dal J, Anton G, Etzerodt A, et al. Targeting the Hemoglobin Scavenger receptor CD163 in Macrophages Highly Increases the Anti-inflammatory Potency of Dexamethasone. Mol Ther. 2012; 20: 1550-8.
12. Krieger M, Herz J. Structures and functions of multiligand lipoprotein receptors-macrophage scavenger receptors and LDL receptor-related protein (LRP). Annu Rev Biochem. 1994; 63: 601-37.
13. Kim SH, Kim JH, You DG, Saravanakumar G, Yoon HY, Choi KY, et al. Self-assembled dextran sulphate nanoparticles for targeting rheumatoid arthritis. Chem Commun. 2013; 49: 10349-51.
14. Ulbrich W, Lamprecht A. Targeted drug-delivery approaches by nanoparticulate carriers in the therapy of inflammatory diseases. J R Soc Interface. 2010; 7: S55-S66.
15. Yang M, Ding J, Zhang Y, Chang F, Wang J, Gao Z, et al. Activated macrophage-targeted dextran-methotrexate/folate conjugate prevents deterioration of collagen-induced arthritis in mice. J Mater Chem B. 2016; 4: 2102-13.
16. Mount C, Featherstone J. Rheumatoid arthritis market. Nat Rev Drug Discov. 2005; 4: 11-2.
17. Khan ZA, Tripathi R, Mishra B. Methotrexate: a detailed review on drug delivery and clinical aspects. Expert Opin Drug Deliv. 2012; 9: 151-69.
18. Torchilin V. Tumor delivery of macromolecular drugs based on the EPR effect. Adv Drug Deliver Rev. 2011; 63: 131-5.
19. Kobayashi H, Watanabe R, Choyke PL. Improving conventional enhanced permeability and retention (EPR) effects; what is the appropriate target? Theranostics. 2013; 4: 81-9.
20. Afshar-Oromieh A, Malcher A, Eder M, Eisenhut M, Linhart HG, Hadaschik BA, et al. Reply to Reske et al.: PET imaging with a [68Ga]gallium-labelled PSMA ligand for the diagnosis of prostate cancer: biodistribution in humans and first evaluation of tumour lesions. Eur J Nucl Med Mol I. 2013; 40: 971-2.
21. Xu W, Ding J, Xiao C, Li L, Zhuang X, Chen X. Versatile preparation of intracellular-acidity-sensitive oxime-linked polysaccharide-doxorubicin conjugate for malignancy therapeutic. Biomaterials. 2015; 54: 72-86.
22. Allen TM, Cullis PR. Drug delivery systems: entering the mainstream. Science. 2004; 303: 1818-22.
23. Ishihara T, Kubota T, Choi T, Higaki M. Treatment of Experimental Arthritis with Stealth-Type Polymeric Nanoparticles Encapsulating Betamethasone Phosphate. J Pharmacol Exp Ther. 2009; 329: 412-7.
24. Choy EHS, Panayi GS. Cytokine Pathways and Joint Inflammation in Rheumatoid Arthritis. New Engl J Med. 2001; 344: 907-16.
25. Choy E. Understanding the dynamics: pathways involved in the pathogenesis of rheumatoid arthritis. Rheumatology. 2012; 51: v3-v11.
26. Feldmann M, Maini SR. Role of cytokines in rheumatoid arthritis: an education in pathophysiology and therapeutics. Immunol Rev. 2008; 223: 7-19.
27. Kotake S, Nanke Y. Effect of TNFalpha on osteoblastogenesis from mesenchymal stem cells. BBA-Gen Subjects. 2014; 1840: 1209-13.
28. Arend WP, Malyak M, Guthridge CJ, Gabay C. Interleukin-1 receptor antagonist: Role in biology. Annu Rev Immunol. 1998; 16: 27-55.
29. Dinarello CA. The IL-1 family and inflammatory diseases. Clin Exp Rheumatol. 2002; 20: S1-13.
30. McInnes IB, Schett G. Cytokines in the pathogenesis of rheumatoid arthritis. Nat Rev Immunol. 2007; 7: 429-42.
31. Kim GW, Lee NR, Pi RH, Lim YS, Lee YM, Lee JM, et al. IL-6 inhibitors for treatment of rheumatoid arthritis: past, present, and future. Arch Pharm Res. 2015; 38: 575-84.
32. Lee H, Lee MY, Bhang SH, Kim BS, Kim YS, Ju JH, et al. Hyaluronate-Gold Nanoparticle/Tocilizumab Complex for the Treatment of Rheumatoid Arthritis. ACS Nano. 2014; 8: 4790-8.